Molecular Orientation in Differently Processed Poly(ethylene terephthalate) Yarns As Studied by ^{13}C 2D CP-MAS NMR

W. Gabriëlse,[†] H. Angad Gaur,[‡] and W. S. Veeman*,[†]

Department of Physical Chemistry, University of Duisburg, 47048 Duisburg, Germany, and Akzo Nobel Central Research, Location Arnhem, P.O. Box 9300, 6800 SB Arnhem, The Netherlands

Received November 14, 1995; Revised Manuscript Received February 13, 1996[⊗]

ABSTRACT: The molecular orientation of a series of differently processed industrial fibers of poly(ethylene terephthalate) (PET) has been investigated by ^{13}C solid-state rotor-synchronized 2D CP-MAS NMR.[1] In addition to the $\langle P_2 \rangle$ order parameters, higher rank order parameters, $\langle P_4 \rangle$ and $\langle P_6 \rangle$, could also be determined. Significant differences in the order parameters were observed as a function of the processing history. The $\langle P_2 \rangle$ order parameters obtained for the range of PET fibers showed a linear relationship with the optical birefringence data. By making plots of the $\langle P_4 \rangle / \langle P_2 \rangle$ and $\langle P_6 \rangle / \langle P_2 \rangle$ ratios corresponding with several types of distributions using a Pearson VII function, the orientation distribution was reconstructed. For the as-spun fibers, relatively high $\langle P_4 \rangle / \langle P_2 \rangle$ and $\langle P_6 \rangle / \langle P_2 \rangle$ ratios were obtained which points to a heavily tailed orientation distribution. The order parameters of the drawn PET fibers agree quite well with the pseudoaffine deformation model.

Introduction

Orientation in polymers is of great technical importance, since the degree of orientation has a strong influence on the physical properties.[2] In the commercial production of poly(ethylene terephthalate) (PET) yarns, the polymer molecules are oriented along the direction of the fiber axis as a result of the spinning process. The as-spun PET yarns can be subjected to an additional drawing process, in which the yarns are stretched at a temperature near the melting temperature of PET. Important process conditions that influence the degree of orientation in PET yarns are the winding speed, the spinning temperature, and the drawing ratio.[3,4] In order to get a better understanding of the way in which process parameters influence the (thermo)mechanical properties, insight into the orientation distribution, which largely determines the yarn properties, is of great importance.

In uniaxially drawn polymers, the molecular orientation distribution is normally described by a function $f(\theta)$, where θ is the angle between a particular molecular fixed axis (e.g., the chain axis) and the axis of preferential orientation (e.g., the fiber axis). When $f(\theta)$ is written as an expansion in Legendre polynomials, $f(\theta)$ is completely defined when all the moments $\langle P_L \rangle$ of the expansion are known. These moments are called the (orientational) order parameters. There exists a variety of methods for studying orientation in polymers. A survey of the most employed methods has been reported by Ward.[5,6] The information obtained with each technique is different. With X-ray diffraction techniques, in principle, all moments of $f(\theta)$ in the crystalline part of the fiber can be determined. However, no orientational information is obtained about the less ordered (amorphous) regions, which mainly determine the physical properties of yarns. Information about the "overall" orientational order can be obtained by birefringence and infrared dichroism measurements. Both techniques, however, provide only the second moment $\langle P_2 \rangle$. More detailed insight into the orientation distribution can already be obtained from polarized laser−Raman spectroscopy, which yields both the second and the fourth moments ($\langle P_2 \rangle$ and $\langle P_4 \rangle$). Besides spectroscopic techniques, the degree of orientation in polymers can also be studied by sonic pulse propagation techniques.[5] Although the theoretical background of this technique has not completely been clarified,[5] it proves to be very useful for studying the relative differences in orientation in fibers.[3,7]

NMR has proved to be a powerful method in studying the orientation in polymers. Various anisotropic NMR interactions like the dipole−dipole interaction, the quadrupolar interaction, and the magnetic shielding interaction can be used to probe molecular orientation. Especially, ^2H experiments are very suitable. Recently, ^2H NMR line-shape studies of deuterated thin PET films provided insight in the orientational order of these materials.[8] In the case of industrially processed fibers, NMR studies are restricted to the naturally abundant ^{13}C or ^1H nuclei. Historically, static ^1H wide line spectra were used to study the orientation. These spectra are not very useful, however, since they have broad structureless shapes due to strong $^1H-^1H$ dipolar interactions between many spins. In principle, the complete orientation distribution function can also be obtained from a line-shape analysis of static (proton decoupled) ^{13}C spectra.[9] However, without enrichment of a specific site, even in polymers with a relative simple chemical composition like PET, poor resolved spectra are obtained due to overlapping of broad chemical shift line shapes.

To overcome these resolution problems, some two-dimensional NMR techniques have been developed, in which the structural and orientational information is separated in two dimensions. The static 2D experiment, in which the sample is flipped through a discrete angle during the mixing time of a 2D exchange experiment, was first applied by Henrichs[25] to characterize the orientation distribution in biaxially drawn industrial PET films. This technique was later named the DECODER experiment.[10−12] Recently, a new version of the DECODER technique which incorporates slow magic angle spinning was reported.[13] This new version eliminates the need for a special NMR probe head, but still there remains the problem of the overlapping of the

[†] University of Duisburg.
[‡] Akzo Nobel Central Research.
[⊗] Abstract published in *Advance ACS Abstracts,* May 1, 1996.

S0024-9297(95)01693-7 CCC: $12.00

broad chemical shift line shapes in systems where more chemically inequivalent sites are present.

Another 2D experiment, which provides a sufficiently high resolution to study the orientation of different segments within a chain, is the 2D rotor-synchronized CP-MAS experiment as developed by Harbison et al.[1] In the ω_2 dimension, the "normal" CP-MAS spectrum is obtained, whereas in the ω_1 dimension a spinning sideband pattern appears which is characteristic for the degree of order in the sample. Theoretically, there is no restriction on the number of order parameters that can be determined with the 2D MAS technique, but in practice, order parameters up to $\langle P_8 \rangle$ are the highest reported (in the case of poly(*p*-phenyleneterephthalamine) (PPTA) fibers).[14] The 2D CP-MAS technique has been applied to a variety of polymer systems, including PET,[1,15] polyethylene,[16] polyamide-6,[17] poly(phenyleneterephthalamine) (PPTA),[14] stretched polycarbonate samples,[18] and liquid-crystalline polymers.[19]

Because of the high resolution and the relatively easy experimental implementation, we used the rotor-synchronized 2D CP-MAS experiment to study the orientation distribution in both as-spun and drawn PET fibers. Special attention was paid to the influence of the chemical shift tensor values used in the fitting analysis. The NMR data are compared with birefringence measurements performed on the same set of samples. Finally, the orientation distribution in PET fibers was reconstructed from the determined moments by making use of a Pearson VII function,[4,30] which covers a wide range of functions including the distribution function that follows from the pseudoaffine deformation model.[2,5]

Theory

I. 2D Rotor-Synchronized CP-MAS Experiment. The theory underlying the rotor-synchronized 2D CP-MAS experiment has been described in detail by Spiess and co-workers.[1,12] We will only briefly outline the main features here.

In the 2D MAS experiment, the carbon-13 chemical shielding anisotropy is used as a tool to study the orientation. A block of fibers is arranged in the rotor, such that the fiber axis, which is also the preferential axis of orientation, makes an angle (β_1) with the rotor axis. Under these conditions, the recorded free induction decay (FID) of an *oriented* sample depends on the position of the rotor (defined by γ_1) at the start of signal detection. This rotor-phase dependence can be exploited to study the degree of orientation of the sample. Harbison et al. designed a 2D experiment in which this γ_1 dependence is sampled at regular steps over a single rotor period in the first time domain (t_1). The FID is recorded during t_2. In practice, it is sufficient to sample over a rotor period in 16 steps. Fourier transformation with respect to t_1 and t_2 gives a two-dimensional spinning sideband spectrum with 16 slices spaced apart by the rotor frequency ω_R in ω_1. The spinning sideband intensities in this 2D spectrum are denoted $I_{M,N}$. The indices M and N indicate the position of a peak shifted $M\omega_R$ in ω_1 and $N\omega_R$ in ω_2 relative to the center band. These intensities are absorptive and can be either positive or negative. The intensities in the ω_2 dimension reflect the chemical structure. The center slice $M = 0$, which contains only positive signals, equals in principle the unsynchronized 1D MAS spectrum of the oriented sample. The intensities in the ω_1 dimension reflect the degree of order: spinning sidebands in higher order slices are obtained for highly ordered systems. For a sample with no molecular orientation, intensities are obtained only in the M = 0 slice. The 2D spectrum thus provides direct qualitative information, whether the sample is ordered or not. For a quantitative analysis, an orientation distribution function must be defined.

II. Analysis of the 2D Spectra. A. Orientation Distribution Function. In uniaxially drawn fibers, it is reasonable to assume that the chains are cylindrically symmetrically distributed around the fiber axis (fiber symmetry). In addition, a cylindrically symmetrical distribution of the chains around their own symmetry axis can be assumed (transverse isotropy). In this case, the orientation distribution function (ODF) can be described with a single angle which represents the angle between a chosen axis along a molecular segment (often the chain axis) and the macroscopic axis of preferential orientation (the fiber axis). The ODF $f(\theta)$ represents the probability of finding a molecular segment between θ and $\theta + \mathrm{d}\theta$. It must therefore obey the normalization condition

$$\int_0^{\pi} f(\theta) \sin\theta \, \mathrm{d}\theta = 1 \tag{1}$$

The shape of the ODF is in many cases a priori unknown. Therefore, the ODF is usually described as an expansion of Legendre polynomials $P_L[\cos(\theta)]$. On the interval $[0, \pi]$, the expansion in Legendre polynomials has the form

$$f(\theta) = \sum_{L=0}^{\infty} \frac{2L+1}{2} \langle P_L \rangle P_L[\cos(\theta)] \qquad L = 0, 2, 4, 6, \cdots \tag{2}$$

The ODF $f(\theta)$ is completely defined when all the moments $\langle P_L \rangle$ of the expansion are known. These moments, which are called the (orientational) order parameters, represent the average values of the Legendre polynomials $P_L[\cos(\theta)]$ and are defined as

$$\langle P_L \rangle = \langle P_L[\cos(\theta)] \rangle = \int_0^{\pi} P_L[\cos(\theta)] \, f(\theta) \sin\theta \, \mathrm{d}\theta \tag{3}$$

The order parameters $\langle P_L \rangle$, which can be determined experimentally, are a quantitative measure of the degree of orientation. They range between 0 for unoriented material and 1 for perfectly oriented material.

B. Determination of the Order Parameters. The order parameters $\langle P_L \rangle$ can be obtained from a linear least-squares fit of calculated "subspectra" intensities $(I_{L,M,N})_{\mathrm{calc}}$ of a specific nucleus to the experimental intensities $(I_{M,N})_{\mathrm{exp}}$ following

$$(I_{M,N})_{\mathrm{exp}} = \sum_{L=0}^{\infty} \frac{2L+1}{2} \langle P_L \rangle (I_{L,M,N})_{\mathrm{calc}} \tag{4}$$

The intensities $(I_{L,M,N})_{\mathrm{calc}}$ represent the subspectra-intensities of a perfectly uniaxially oriented system weighted with the Legendre polynomials $P_L[(\cos\theta)]$. In principle, it is possible to determine the order parameters of each chemical inequivalent carbon site in PET, with the exception of the protonated aromatic carbons, since two sites of these carbons with a different tensor orientation relative to the chain axis exist, which are not resolved in the ^{13}C spectrum. Also, the ethylene carbon is not very useful if we want to have an accurate determination of the order parameters, due to the limited number of spinning sidebands obtained in the

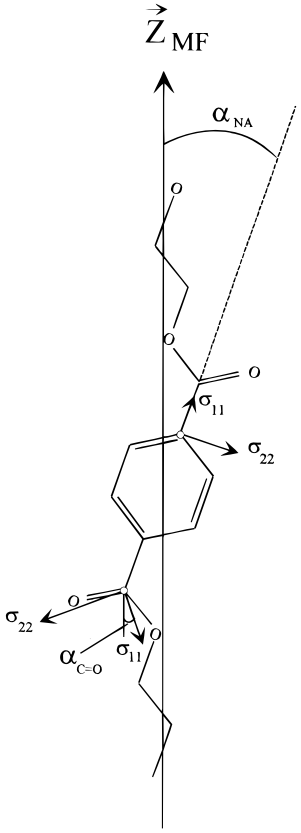

Figure 1. Schematic representation of two chemical shift tensor orientations in PET.

2D spectrum. Therefore, in PET, the carbonyl and the nonprotonated aromatic carbons remain.

C. Chemical Shift Tensors in PET. In this paragraph, we would like to address an important issue with respect to the analysis of the 2D spectra in terms of order parameters. Accurate calculation of $(I_{L,M,N})_{calc}$ requires an accurate knowledge of the principal values (σ_{11}, σ_{22}, σ_{33}) of the chemical shift tensor σ and the Euler angles (α_0, β_0, γ_0) that relate the principal axis system (PAS) of σ to the molecular frame (MF) of reference. The MF can in principle be arbitrarily chosen with respect to the molecule. We choose the chain axis as the z axis of the MF (Z_{MF}) as indicated in Figure 1. Figure 1 shows a schematic representation of the trans conformation of PET, which is the conformation of PET in the crystalline regions.[21,22] Since there are no single crystals of PET, the tensor orientation relative to the molecular axes can only be guessed from single crystal studies of comparable compounds[23] or must be determined by another method.[24] We will discuss both the tensor orientation of the nonprotonated aromatic carbon and of the carbonyl carbon in PET.

Nonprotonated Aromatic Carbon. This nucleus has the advantage over the carbonyl carbon in that the orientation of the PAS relative to the local aromatic ring structure is well-defined. It is assumed that the principal axis σ_{33} is directed perpendicular to the aromatic ring plane, σ_{11} lies along the C−C axis, and σ_{22} lies in the aromatic ring plane and points in the direction perpendicular to σ_{11}, as indicated in Figure 1. The additional parameter that is needed to characterize the orientation of PAS in the MF is the angle α_{NA} between the aromatic para axis and the chain axis (Z_{MF}). In the crystalline regions, this angle can be determined from wide angle X-ray diffraction techniques (WAXS). From the reported atomic coordinates of the unit cell of PET,

Table 1. Experimental and Literature Values of the Chemical Shift Tensor Principal Values of the Nonprotonated Aromatic Carbon in PET and Euler Angles That Relate the PAS to the MF of Reference

σ_{11}, ppm	σ_{22}, ppm	σ_{33}, ppm	α_{NA}, deg	β_{NA}, deg	γ_{NA}, deg	ref
		Experimental Values				
−233 ± 1	−142 ± 2	−28 ± 1	23 ± 2[a]	90	0	
			20 ± 1[a]	90	0	
		Literature				
−228 ± 3	−146 ± 3	−31 ± 3	18 ± 4	90	0	11
−230	−145	−31				25

[a] The values 23 ± 2° and 20 ± 1° were obtained, respectively, for drawn and as-spun PET fibers.

angles of 24[21] and 19°[22] for α_{NA} can be calculated. The latter value should be more accurate, since this value is calculated from a more accurate determination of the crystal structure of PET using full pattern X-ray diffraction refinement. Chmelka et al.[11] determined a value of 18 ± 4° based on simulations of their NMR DECODER spectra. As was reported in an earlier paper,[24] it is possible to determine both the principal values and the tensor orientation from the best fit to the 2D spectrum. In these simulations, the Euler angle β_{NA}, which rotates the σ_{33} axis into the aromatic ring plane, was set fixed at an angle of 90°. The Euler angle γ_{NA}, which in principle can have any value between 0 and 360° due to the symmetry of the system,[12] was set to 0. The chemical shift principal values were varied simultaneously with the variation of the Euler angle α_{NA} in order to obtain the best fit. For the whole range of fibers studied, we found that α_{NA} ranged between 22 and 25° for drawn yarns and between 20 and 21° for the as-spun fibers, yielding mean values of respectively 23 ± 2 and 20 ± 1°. The accuracy of this method is demonstrated by the small standard deviations. Both values agree well with the reported X-ray values mentioned above.[21,22] The Euler angles that are used for the calculation of the order parameters are summarized in Table 1. It should be noted that the α_{NA} value we find represents an average value of both amorphous and crystalline regions. In the amorphous phase, also gauche conformations of PET occur, which might account for the observed difference in α_{NA} between drawn and as-spun fibers, which differ in crystallinity. Although the observed differences between the as-spun and drawn fibers seem small, we found that α_{NA} is shifted to lower values when the fraction of amorphous material increases.

The principal values of the nonprotonated aromatic carbon used in our simulations are also listed in Table 1. These values are also obtained from the best fit to the 2D spectrum.[24] They represent the mean values of the series of samples. Also here, the small standard deviation demonstrates the accuracy of this method. These values differ slightly from literature values, which are listed in the same table.[11,25] In principle, the principal values can also be obtained from a Herzfeld and Berger analysis[26] of a ^{13}C spinning sideband spectrum obtained from a powdered form of the sample. However, as reported in another paper,[24] these values differed 5−10 ppm in magnitude from the principal values obtained from the 2D spectrum. We assume that the Herzfeld and Berger analysis might yield wrong estimates of the principal values due to macroscopic orientation of the fibers in the rotor. It should be emphasized that only with the values obtained from the 2D spectrum were realistic order parameters obtained

Table 2. Process and Structure Parameters of the PET Yarns Studied. The Values for *H* and *Z* Yield a Pearson VII Function that Corresponds within the Error with the Determined Order Parameters

sample	winding speed, m/min	draw ratio	V_C	Δn	Order parameters $\langle P_2\rangle$ (±0.02)	$\langle P_4\rangle$ (±0.03)	$\langle P_6\rangle$ (±0.05)	Reconstructed Pearson VII *H*, deg	Z
				As-Spun					
vis21Q600	600	0	0.016	0.003	0.0	0.0	0.0	∞	
visQ4200	4200	0	0.166	0.080	0.37	0.27	0.23	1.0[a]	0.54[a]
C5500D-spinsel	5500	0	0.238	0.117	0.49	0.37	0.26	4.6 ± 2.6	0.82 ± 0.15
				Drawn					
C500D-10%	500	6.0	0.356	0.200	0.73	0.57	0.48	6.5 ± 3.7	1.18 ± 0.09
FKRIO47AN004	2000	2.6	0.371	0.189	0.65	0.48	0.36	9.0 ± 3.7	0.97 ± 0.11
FKRIO47AN005	2000	3.0	0.368	0.192	0.65	0.44	0.38	6.1 ± 3.6	0.62 ± 0.12
FKRIO47DN001	3500	1.7	0.366	0.170	0.64	0.49	0.34	9.6 ± 3.4	0.79 ± 0.12
FKRIO47DN006	3500	2.2	0.390	0.190	0.69	0.51	0.34	15.8 ± 6.1	1.38 ± 0.16
C5500D-10%	5500	1.6	0.361	0.180	0.68	0.52	0.32	17.3 ± 5.3	1.42 ± 0.16

[a] The order parameters of this yarn actually fall just outside of the Pearson VII range: the values represent the best solution that comes near the values of the order parameters.

which were in good agreement with birefringence data and order parameters obtained from polarized laser Raman measurements.[28]

Carbonyl Carbon. From single-crystal studies, it has been shown that for carbonyl and carboxyl carbons, the σ_{33} axis is directed parallel or nearly parallel to the normal of the O−C−O plane. The directions of the principal axes σ_{11} and σ_{22}, however, are very sensitive to the local structure around the C═O group.[23] Chmelka et al.[11] estimated from their simulation of DECODER spectra of PET an angle of 18 ± 7° between the σ_{11} axis and the chain axis (this angle is denoted $\alpha_{C=O}$ as indicated in Figure 1). In contrast to the calculations of the nonprotonated aromatic carbon discussed above, the quality of the 2D fit for the carbonyl carbon was almost independent of the carbonyl tensor orientation. Also here, the chemical shift principal values were varied simultaneously with the variation of $\alpha_{C=O}$. Apparently, a change in the chemical shift tensor orientation as defined by $\alpha_{C=O}$ does not lead to a significant change in the *relative* intensities of the calculated subspectra, yielding a better fit. This may be due to the fact that the carbonyl tensor is almost axially symmetric. On the other hand, a change in $\alpha_{C=O}$ yields another set of order parameters, indicating a change in the *absolute* intensities of the subspectra. By choosing a range of $\alpha_{C=O}$ values between 0 and 20°, we determined the corresponding order parameters for each value of $\alpha_{C=O}$. From these order parameters, we can conclude the following: (i) The order parameter $\langle P_2\rangle$ is not very dependent on $\alpha_{C=O}$ and is always significantly smaller than the $\langle P_2\rangle$ of the aromatic ring. This would suggest a lower ordering of the C═O group in comparison with the aromatic ring. Although we did not investigate this point in more detail, we suppose that this "lower" ordering for the carbonyl group might be due to motions of the carbonyl group at the time scale of the increment time in t_1, which is about 14 μs (∼70-kHz motions). In the analysis of the 2D spectra, we did not account for these motional effects. (ii) The order parameters $\langle P_4\rangle$ and $\langle P_6\rangle$ are strongly dependent on $\alpha_{C=O}$, in such a way that large values of $\alpha_{C=O}$ (≥10°) lead to unrealistically high values of $\langle P_4\rangle$ and $\langle P_6\rangle$. On the basis of the abovementioned points, we preferred to use the nonprotonated aromatic carbon for the determination of the order parameters from the 2D spectra.

Experimental Section

Samples. The melt-spun PET fibers were provided by Akzo Nobel Central Research, Arnhem, The Netherlands. In this study, both as-spun and drawn yarns are studied in order to cover a broad range of physical structures. The fibers are given in Table 2 together with their winding speed and draw ratio. For the 2D experiments, the PET samples were carefully prepared such that the angle between the yarn axis and the rotor axis is 60°. It was experimentally found that this angle gives the largest number of spinning sideband intensities in the ω_1 dimension. Deviations of this angle due to misalignment of the fibers during sample preparation are smaller than 2°. The fibers were split into strands of 300 dtex (1 tex = 1 g/1000 m) and parallel wound on a flat spool, forming a layer. The as-spun and drawn fibers are wound under a tension of respectively 0.5 cN/tex (15 g) and 2 cN/tex (60 g). Three to four layers were wound on top of each other. These layers are held together by a commercial epoxy glue (UHU) which is smeared in between each layer. The glue (which only gives intensities in the center slice $M = 0$ of the 2D spectrum) was selected to give little signal overlapping with the PET spectrum. From the obtained PET sheet, a strip of dimension of 4.5 × 10 mm is cut at an angle of 60° to the fiber direction. Five to six of these strips are parallel glued together to form blocks of 4.5 × 4.5 × 10 mm. These samples are loaded in a rotor of 7-mm outer diameter. For stable spinning, the rotor is balanced by filling the empty spaces with a fine powder (Al_2O_3).

NMR Spectroscopy. The NMR measurements were performed at a Bruker ASX400 spectrometer operating at 400 MHz for protons. A double-bearing CP-MAS probe was used with 7-mm spinners. The rotor speed was 4.4 kHz. The standard pulse sequence as designed by Harbison et al.[1] was used. The down edge of the rotor signal triggers the start of the pulse sequence. After a constant waiting time t_0 of 10 μs, the evolution time $t_1$was incremented in 15 steps of $^1/_{16}$ of the rotor period. The ^{1}H and ^{13}C 90° pulse lengths were 5 μs. FID's taken at different times t_1 were obtained by repeatedly cycling through the 16 t_1 times, for each time adding at least 200 FID's. Further experimental parameters are recycle delay, 2 s, and cross-polarization time, 3 ms. All spectra were recorded at room temperature. As described in an earlier paper,[24] the measured serial file containing 16 FID's was used to construct a serial file of 128 FID's. Fourier transformation of this enlarged serial file yields much cleaner spectra. The data fitting for the calculation of the order parameters was performed on a Convex C220 computer. The original software was supplied by Spiess and co-workers. As described before,[24] this software was modified such that the magnetic shielding tensor principal values and Euler angles could be varied.

Results and Discussion

I. Spectra. As an example, two ^{13}C 2D rotor-synchronized CP-MAS spectra of a PET yarn wound at a high speed (5500 m/min, draw ratio 1.6) and an as-spun yarn wound at a low spinning speed (600 m/min) are shown in, respectively, Figure 2a and 2b. The centerband signal of each nucleus is indicated in Figure 2a. The glue signals are marked by an x. Both spectra

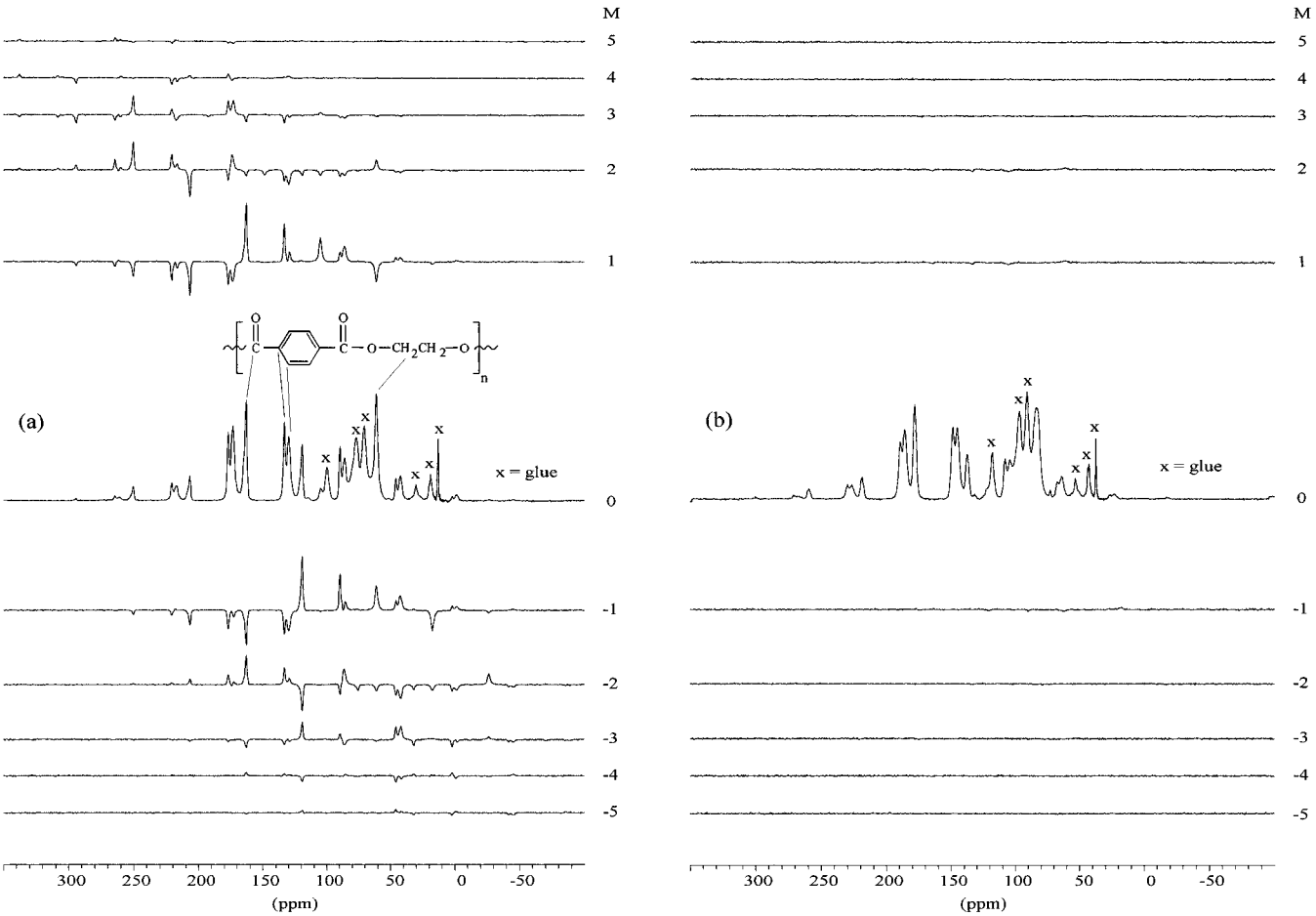

Figure 2. ^{13}C rotor-synchronized 2D CP-MAS spectra of (a) a drawn PET yarn (spinning speed = 5500 m/min, draw ratio = 1.6) and (b) an as-spun PET yarn wound at a spinning speed of 600 m/min.

reveal a clear difference in molecular order. Figure 2a shows a spinning sideband pattern with intensities extending up to $M = 5$, whereas Figure 2b shows no clearly visible spinning sidebands in the ω_1 dimension. It is noted that a fit of the intensities in the $M = 5$ slice, which originate from the carbonyl and aromatic nuclei, requires in addition to the $\langle P_2 \rangle$ and $\langle P_4 \rangle$ order parameters a higher rank order parameter, $\langle P_6 \rangle$.

II. Order Parameters. The order parameters obtained for different PET samples are given in Table 2. As mentioned before these order parameters are calculated for the aromatic ring. For comparison with other data, Table 2 contains also the volume fraction crystallinity data (V_C), as determined from a combination of WAXS and density measurements,[3,4] and the optical birefringence data (Δn). The indicated inaccuracy of the order parameters represents the error estimated from the inaccuracy of the tensor orientation and principal values. For all yarns, except the as-spun fiber wound at a low speed (vis21Q600), order parameters up to $\langle P_6 \rangle$ could be determined. Addition of an extra order parameter, $\langle P_8 \rangle$, in the regression analysis did not improve the quality of the fit and was therefore left out. For all samples, the order parameters tend to decrease to zero, as we proceed to higher rank order parameters. This behavior is consistent with the general idea of a monotonically decaying orientation distribution function. Significant differences in the degree of order are observed amongst the series of PET yarns as a function of the processing parameters. The as-spun yarn drawn at a low speed (600 m/min) shows no orientation ($\langle P_2 \rangle = 0$), which is in agreement with the almost zero optical birefringence. The degree of order increases with the winding speed. For the yarn wound at the highest speed of 5500 m/min, a $\langle P_2 \rangle$ value of almost 0.5 was obtained. It is interesting to note that the $\langle P_4 \rangle$ and $\langle P_6 \rangle$ values of the as-spun yarns are remarkably high relative to the $\langle P_2 \rangle$ values. These high ratios for $\langle P_4 \rangle / \langle P_2 \rangle$ and $\langle P_6 \rangle / \langle P_2 \rangle$ show that the orientation distribution in these yarns is not a simple Gaussian, as will be discussed in more detail in the next section. The highest order parameters are obtained for the drawn yarns. Depending on the draw ratio and the initial spinning speed, the $\langle P_2 \rangle$ values ranged between 0.64 and 0.73.

A good test for the reliability of the order parameters, or at least for the $\langle P_2 \rangle$ values, is the comparison of the $\langle P_2 \rangle$ order parameters with the optical birefringence Δn. To a first-order approximation[5] the second moment $\langle P_2 \rangle$ is linearly related to Δn via

$$\Delta n = \Delta n_{\max} \frac{1}{2}(3\langle \cos^2 \theta \rangle - 1) = \Delta n_{\max} \langle P_2 \rangle \qquad (5)$$

where $\Delta n_{\max}$ is the intrinsic birefringence at full orientation ($\langle P_2 \rangle = 1$). The experimental relationship between our $\langle P_2 \rangle$ values and the birefringence data is given in Figure 3. Although our samples do not cover the whole orientation range, a linear relationship is clearly observed. The dashed line in Figure 3 represents a linear regression fit of the data. From the slope, an intrinsic birefringence value of 0.272 ± 0.018 is obtained. Although slightly larger, this value is in good agreement with the recently reported value of 0.244 ±

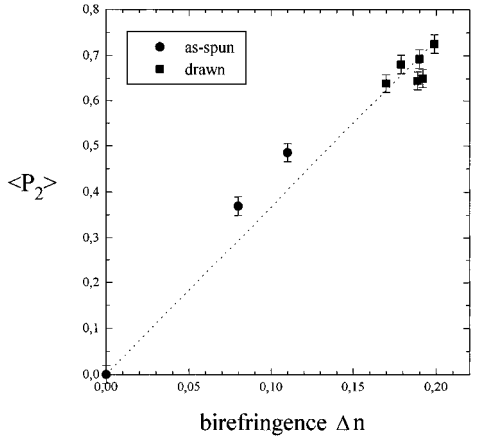

Figure 3. Experimental relationship between the $\langle P_2 \rangle$ order parameter determined with NMR and the optical birefringence Δn.

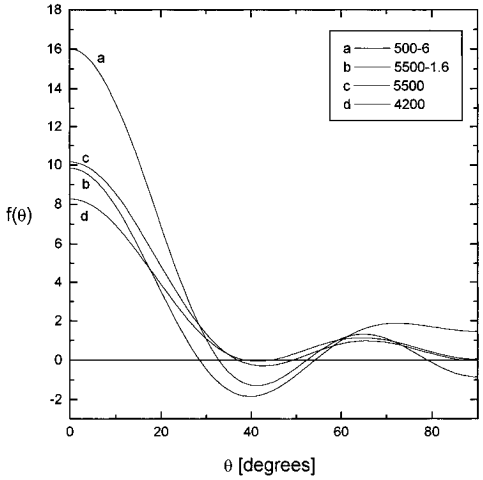

Figure 4. Expansion in Legendre polynomials based on measured order parameters $\langle P_2 \rangle$, $\langle P_4 \rangle$, and $\langle P_6 \rangle$, as given in Table 2.

0.010 obtained from a Raman study of as-spun PET fibers.[27] This means that the $\langle P_2 \rangle$ order parameters obtained with NMR agree well with those obtained with Raman measurements. Comparisons between both methods are allowed since in the Raman study the same segment (benzene ring vibration at 1615 cm^{-1}) was used for the determination of the order parameters.

It should be recognized that the observed Δn in eq 5 represents the total polarizability anisotropy which is constituted of the individual polarizability anisotropies of different molecular groups in PET, whereas the $\langle P_2 \rangle$ order parameter we measure reflects the orientation distribution of a specific segment of the chain, in our case the aromatic ring. The observed linear relationship therefore indicates that the orientation distribution of the aromatic rings give a good representation of the average orientation distribution of the chains. This can be well understood, since the conjugated π-electrons in the benzene group give the main contribution to the total optical anisotropy.

III. Orientation Distribution in PET Fibers. A. Pearson VII Function. The overall orientation distribution is not completely known until all of the order parameters that are not zero are known. We have shown that for PET fibers, we can determine the second, the fourth, and the sixth moment of the distribution. From the data given in Table 2, $\langle P_6 \rangle$ is obviously not very small, except for the amorphous sample. It is therefore reasonable to assume that the unknown higher rank order parameters ($L > 6$) are not zero. The orientation distribution is therefore not completely defined by $\langle P_2 \rangle$, $\langle P_4 \rangle$, and $\langle P_6 \rangle$. Figure 4 shows the distribution functions of four PET yarns based on the order parameters given in Table 2. The samples are denoted by their winding speeds and drawing ratios. Since $f(\theta)$ must be positive for each value of θ, these functions generated from $\langle P_2 \rangle$, $\langle P_4 \rangle$ and $\langle P_6 \rangle$ are not realistic. The "oscillations" in the tail of the distribution are due to missing higher moments. It is obvious that we have to find another way to reconstruct the orientation distribution from the known moments. When no assumptions can be made about the shape of the distribution, one might use the maximum information−entropy formalism[28,29] in order to obtain the "most probable" distribution based on the minimal information provided, the moments of the distribution. However, some reasonable assumptions with respect to the profile of the distribution can be made, considering the forming and drawing process of the fibers: (i) The maximum of the distribution must lie at $\theta = 0°$. (ii) The distribution can be assumed to be monotonously decaying on the interval $[0,\pi/2]$.

One might argue that the PET fibers are semicrystalline and that, therefore, the orientation distribution is bimodal and must be described by a sum of at least two distribution functions. In fact, NMR relaxation measurements on PET yarns pointed to the existence of three motionally different regions:[32] crystalline, rigid (oriented) amorphous, and mobile (disordered) amorphous. Although the distribution might be bimodal or three modal, we first try to describe the overall distribution with a single function in which we do not restrict ourselves to a Gauss or a Lorentz function but allow the distribution function to adapt a wide range of profiles using the Pearson VII function.[4,30] The Pearson VII function can be formulated in the following way:

$$f(\theta) = \frac{I_0}{\left[1 + \left(\frac{2 \sin \theta}{H}\right)^2 (2^{2-Z} - 1)\right]^{1/(2-Z)}} \qquad (6)$$

where I_0 represents the maximum intensity at $\theta = 0$, H is the half-width of the distribution,[31] and Z governs the shape of the function at the tail. We will call this shape parameter the "tailing factor" of the function, which can range between the values 0 and 2. The effect of the tailing factor on the distribution is illustrated in Figure 5, where plots of the function with the same half-width ($H = 20$) are given for different values of Z. These plots show that the tailing of the distribution increases with decreasing Z. This plot shows an important advantage of the Pearson VII function: the half-width and the tail of the distribution can be varied independently, a property not possessed by more conventional functions such as Gauss and Lorentz functions. As a matter of fact, the latter functions can be described by the Pearson VII function for special values of the shape parameter Z. For $Z = 1$, the Pearson VII function gives a Lorentz distribution:

$$f(\theta) = \frac{I_0}{1 + \left(\frac{2 \sin \theta}{H}\right)^2} \qquad (7)$$

For the limit of $Z \rightarrow 2$, the function becomes a Gaussian:

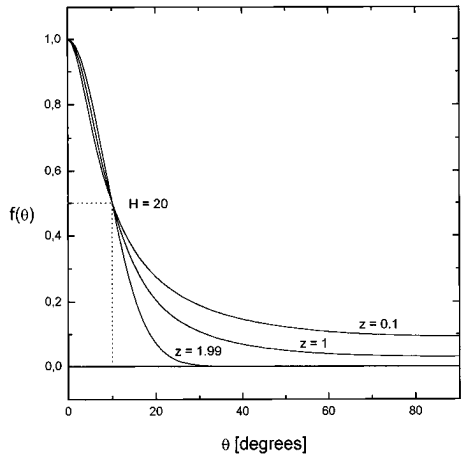

Figure 5. Example of three Pearson VII functions with a half-width $H = 20$ and different tailing factors Z.

$$f(\theta) = I_0 \exp\left(\frac{-(\sin^2 \theta)}{2\sigma^2}\right) \tag{8}$$

where $\sigma = H/2\sqrt{2 \ln 2}$ is the root-mean-square width of the Gaussian. Due to these favorable properties, the Pearson VII function was applied before as a fitting function to adjust X-ray line shapes.[4] It is noted that the Pearson VII function does not originate from any physical model. However, it gives an exact description of the distribution function that follows from the pseudoaffine deformation model. The affine deformation model[5,6,20] is one of the best known theoretical models for predicting orientation in polymers which occurs during a drawing process. The polymer is supposed to be an aggregate of rodlike (transverse isotropic) units rotating toward the draw direction on drawing. The orientation of a single unit is defined by the angle θ between the symmetry axis and the draw direction, as illustrated in Figure 6. It is assumed that on drawing, the symmetry axes of the units rotate in the same way as the lines joining pairs of points on the macroscopic body, which deforms uniaxially at constant volume (see Figure 6). More precisely, this model was named the "pseudoaffine" deformation scheme by Ward,[5,6] since it does not incorporate an elongation of the units on deformation. It is clear that in the pseudoaffine model, which was first proposed by Kratky,[33] the orientation develops initially more rapidly as a function of the extension ratio than in the affine model.[5] The orientation distribution function $f(\theta)$ that results from a pseudoaffine deformation of an isotropic sample which is extended from length L to length λL by the factor λ (the draw ratio) is given by[28]

$$f(\theta) = \frac{\lambda^3}{[1 + (\lambda^3 - 1)\sin^2 \theta]^{3/2}} \tag{9}$$

This Pearson VII function gives an exact description of the pseudoaffine distribution for $Z = {}^4/_3$ and $H = 2\sqrt{(2^{2/3} - 1)/(\lambda^3 - 1)}$. This relationship was first pointed out by van Wijk.[34]

B. Relation between Order Parameters and Pearson VII. To get a feeling for the relation between the distribution function and order parameters, we plotted the ratios between order parameters for several types of Pearson VII distributions together with the experimental values, as shown in Figure 7. In addition

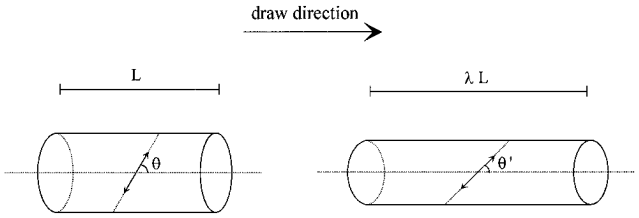

Figure 6. Schematic representation of the pseudoaffine deformation model.

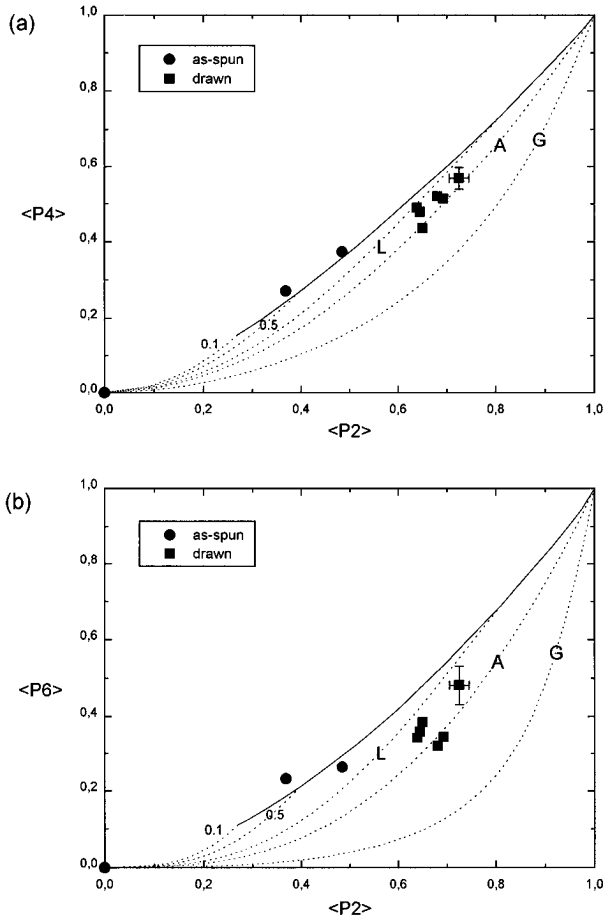

Figure 7. (a) $\langle P_4\rangle/\langle P_2\rangle$ and (b) $\langle P_6\rangle/\langle P_2\rangle$ plots showing the experimental data and theoretical curves corresponding with a range of moments that can be described with the Pearson VII function. The dashed lines correspond with different values of Z, i.e., $Z = 0.1$, $Z = 0.5$, $Z = 1$ (Lorentz, L), $Z = {}^4/_3$ (pseudoaffine, A), and $Z = 1.99$ (Gauss, G). The solid upper curve represents a sharp peaked distribution ($H = 0.1$) for different values of Z ($0 < Z < 2$).

to the $\langle P_4\rangle/\langle P_2\rangle$ plot as reported before by other authors for several uniaxial distributions,[28,35] the determination of $\langle P_6\rangle$ allows us to also make a $\langle P_6\rangle/\langle P_2\rangle$ plot. The addition of the sixth moment can give a more confident picture of the distribution than that derived only from the $\langle P_4\rangle/\langle P_2\rangle$ plot. For visual clarity, the error margins of the experimental data (see Table 2) are indicated for only a single data point. The moments corresponding with the distribution $f(\theta)$ are calculated via

$$\langle P_L\rangle = \frac{\int_0^\pi f(\theta) P_L(\cos\theta) \sin\theta \, d\theta}{\int_0^\pi f(\theta) \sin\theta \, d\theta} \tag{10}$$

Two extreme situations of the state of order are the isotropic distribution ($\langle P_2\rangle = \langle P_4\rangle = \langle P_6\rangle = 0$) and perfect

orientation at $\theta = 0°$ ($\langle P_2\rangle = \langle P_4\rangle = \langle P_6\rangle = 1$). The dashed curves show the range of moments that correspond with several types of distributions in between these extremes, including a Gaussian (G), a pseudoaffine distribution (A), a Lorentzian (L), and distributions with an even higher tailing factor ($Z = 0.5$, $Z = 0.1$). The upper solid curve corresponds with Pearson VII functions with a half-width of 0.1° and various values of Z ($0 < Z < 2$). This curve shows that even for narrow distributions ($H = 0.1$), the order parameters decrease significantly when the tailing factor increases. All combinations of moments that fall within the upper and lower curves can be described by a Pearson VII function.

Obviously the experimental data in the $\langle P_4\rangle/\langle P_2\rangle$ plot fall in the same range as in the $\langle P_6\rangle/\langle P_2\rangle$ plot, which means that the distribution derived from the second and the fourth moments is confirmed by the sixth moment of the distribution. The experimental data show clearly that the overall orientation distribution of both as-spun and drawn yarns cannot be described by a Gaussian. For the drawn yarns, the data fall in the regime between the Lorentzian and pseudoaffine curve. The data of the as-spun fibers fall in a different region: they are located at the upper boundary of the Pearson VII regime. In fact, the order parameters of the sample visQ4200 fall just outside of the Pearson VII range. We used a computer program that made use of an iterative fitting routine in order to obtain the set of H and Z values that gives the best match with the determined moments. The results are summarized in Table 2. The errors correspond with the uncertainty in the order parameters. The results show that the order parameters of the as-spun fibers wound at high speeds (4200, 5500 m/min) correspond with a Pearson VII distribution with a smaller half-width and a larger tailing factor (lower Z value) than that of the drawn yarns.

As an example, we plotted in Figure 8 the distributions of two fibers: Figure 8a shows the distribution of the as-spun PET fiber wound at a speed of 5500 m/min and Figure 8b that of the fiber that is drawn from the as-spun fiber wound at 5500 m/min with a draw ratio of 1.6. Both functions are normalized according to eq 1. We believe that the narrow part of the distribution in Figure 8a can be attributed to the crystalline fraction. Previous studies of the formation of crystals during spinning,[3,4] showed that at the onset of a spinning speed of about 2000 m/min, crystals will be formed, which are highly oriented with respect to the fiber axis. As indicated in Table 2, the volume fraction crystallinities of the as-spun fibers are 16.6% (4200 m/min) and 23.8% (5500 m/min). The broad part of the distribution ("the tailing") can be attributed to the disordered amorphous phase. These assignments are supported by the fractions of material that contribute to both parts of the distribution. Integration shows that 27 ± 5% of the material contributes to the narrow part (<10°), which is within the error consistent with the volume fraction crystallinity of 23.8% of this sample. We assume that the broader half-width in Figure 8b reflects the distribution of the crystals *and* that of the oriented amorphous phase. Also, this is consistent with calculations that show that at least 60% of the material contributes to the narrow part of the distribution, which is significantly larger than the volume fraction crystallinity (35%) of this sample. From these observations, we can conclude that the disordered amorphous phase of the as-spun fiber gets oriented upon hot drawing.

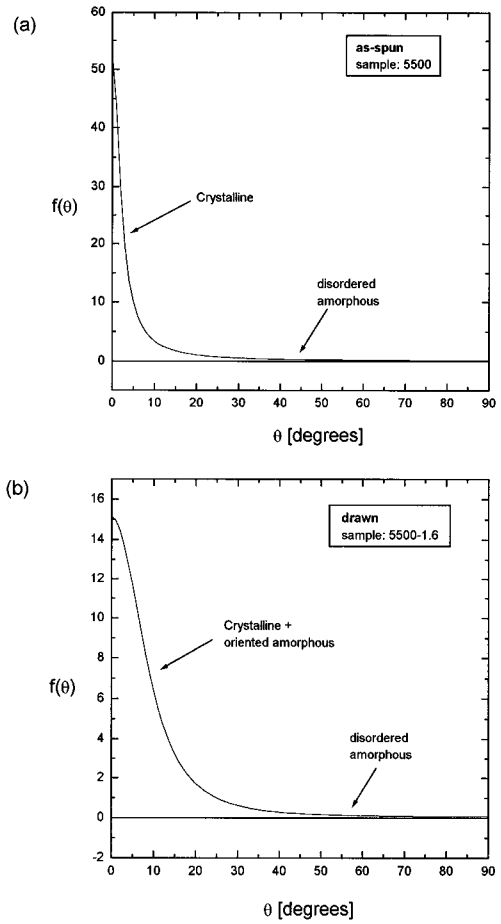

Figure 8. Reconstructed Pearson VII orientation distribution for (a) an as-spun PET fiber (5500) and (b) a drawn PET fiber (5500−1.6).

The observation of distinctive narrow and broad components in the orientation distribution of PET fibers, which is shown to be most profound for the as-spun PET fibers, is in agreement with the distribution functions reconstructed from DECODER NMR spectra of PET fibers as reported by Chmelka et al.[11] Their distributions yield a similar set of order parameters with relatively high $\langle P_4\rangle/\langle P_2\rangle$ and $\langle P_6\rangle/\langle P_2\rangle$ ratios. It is noted, however, that in the analysis of the 2D DECODER spectra, the ODF was extracted from the O−CH_2 resonances, whereas we determine the order parameters of the aromatic ring. Since the PET molecule is not a rigid segment, the orientation of different segments might not be the same.

We finally like to point to the interesting fact that the order parameters of the drawn yarns seem to agree well with the pseudoaffine deformation model. It should be emphasized that the affine deformation model starts from an isotropic orientation distribution. With the exception of the yarn wound initially at a low speed of 500 m/min (C500D-10%), all other drawn yarns originate from as-spun fibers wound at higher winding speeds of 2000−5500 m/min. It has been shown above that the orientation distribution in these as-spun yarns is clearly not isotropic and is shown to be nonpseudoaffine. It is therefore surprising that the orientation distribution in the yarns drawn from the as-spun fibers seems to agree quite well with the pseudoaffine deformation model, which starts from an isotropic distribution. This would imply that the initial nonpseudoaffine orientation distribution gets drawn toward a pseudoaffine distribution upon uniaxial stretching. A more

systematic study of these observed trends is currently going on in our laboratory.

Conclusions

It has been shown that with the ^{13}C 2D rotor-synchronized solid state NMR technique, physically acceptable and reliable order parameters were obtained for a range of PET fibers. The assumed linear relationship between the $\langle P_2 \rangle$ order parameters and the optical birefringence Δn was demonstrated. This relationship was in quantitative agreement with Raman studies of as-spun PET fibers. The molecular orientation in PET yarns is strongly dependent on the processing history. The as-spun fiber wound at a low speed of 600 m/min shows no orientation. At higher winding speeds, the orientation increases. Since the NMR method also provides the higher rank $\langle P_4 \rangle$ and $\langle P_6 \rangle$ order parameters in addition to the $\langle P_2 \rangle$ order parameters, more detailed information about the orientation distribution can be obtained. The overall orientation distribution in as-spun PET fibers differs from that of drawn PET fibers. In as-spun fibers, the ratio between the order parameters indicates a heavily tailed orientation distribution, which reflects the superposition of a narrow (crystalline) component and a broad (amorphous) component. The order parameters obtained for drawn yarns seem to agree quite well with a pseudoaffine distribution function, indicating a substantial degree of order in the amorphous phase.

Acknowledgment. We gratefully acknowledge H. M. Heuvel for his encouraging support of this work from the very beginning and for providing the X-ray and birefringence data of the PET samples. We also thank A. P. de Weijer for developing some very useful computer programs used in this work and R. J. van Wijk for many clarifying and stimulating discussions that contributed substantially to the interpretation of the results.

References and Notes

(1) Harbison, G. S.; Vogt, V.; Spiess, H. W. *J. Chem. Phys.* **1987**, *86* (3), 1206.
(2) Ward, I. M. *Mechanical properties of Solid Polymers*, 2nd ed.; John Wiley & Sons: Chichester, 1983.
(3) Heuvel, H. M.; Huisman, R. *J. Appl. Polym. Sci.* **1978**, *22*, 2229.
(4) Huisman, R.; Heuvel, H. M. *J. Appl. Polym. Sci.* **1989**, *37*, 595.
(5) Ward, I. M. *Structure and properties of oriented polymers*; Applied Science: London, 1975.
(6) Ward, M. *Adv. Polym. Sci.* **1985**, *66*, 81.
(7) Heuvel, H. M.; Lucas, L. J.; van den Heuvel, C. J. M.; de Weijer, A. P. *J. Appl. Polym. Sci.* **1992**, *45*, 1649.
(8) Röber, S.; Zachmann, H. G. *Polymer* **1992**, *33* (10), 2061.
(9) Hentschel, R.; Schlitter, J.; Sillescu, H.; Spiess, H. W. *J. Chem. Phys.* **1978**, *68*, 556.
(10) Schmidt-Rohr, K.; Hehn, M.; Schaefer, D.; Spiess, H. W. *J. Chem. Phys.* **1992**, *97* (4), 2247.
(11) Chmelka, B. F.; Schmidt-Rohr, K.; Spiess, H. W.*Macromolecules* **1993**, *26*, 2282.
(12) Schmidt-Rohr, K.; Spiess, H. W. *Multidimensional Solid-State NMR and Polymers*; Academic: London, 1994, Chapter 12.
(13) Lewis, R. H.; Long, H. W.; Schmidt-Rohr, K.; Spiess, H. W. *J. Magn. Reson. Ser. A* **1995**, *115*, 26.
(14) Wilhelm, M.; Féaux de Lacroix, S.; Titman, J. J.; Schmidt-Rohr, K.; Spiess, H. W. *Acta Polym.* **1993**, *44*, 279.
(15) Tzou, D. L.; Desai, P.; Abhiraman, A. S.; Huang, T. H. *J. Polym. Sci.: Part B: Polym. Phys.* **1995**, *33*, 63.
(16) Tzou, D. L.; Huang, T. H.; Desai, P.; Abhiraman, A. S. *J. Polym. Sci.: Part B: Polym. Phys.* **1993**, *31*, 1005.
(17) Tzou, D. L.; Spiess, H. W.; Curran, S. *J. Polym. Sci.: Part B: Polym. Phys.* **1994**, *32*, 1521.
(18) Vogt, V. D.; Dettenmaier, M.; Spiess, H. W.; Pietralla, M. *Colloid Polym. Sci.* **1990**, *268*, 22.
(19) Titman, J. J.; Tzou, D. L.; Féaux de Lacroix, S.; Boeffel, C.; Spiess, H. W. *Acta Polym.* **1994**, *45*, 204.
(20) Kuhn, W.; Grün, W. *Kolloid-Z.* **1942**, *101*, 248.
(21) Daubeny, R. de P.; Bunn, C. W.; Brown, C. J. *Proc. R. Soc. London, Ser. A* **1954**, *226*, 531.
(22) Fu, Y.; Busing, W. R.; Yin, Y.; Affholter, K. A.; Wunderlich, B. *Macromolecules* **1993**, *26*, 2187.
(23) Veeman, W. S. *Prog. NMR Spectrosc.* **1984**, *16*, 193.
(24) Gabriëlse, W.; van Well, H. F. J. M.; Veeman, W. S. *Solid State NMR*, in press.
(25) Henrichs, P. M. *Macromolecules* **1987**, *20*, 20.
(26) Herzfeld, J.; Berger, A. E. *J. Chem. Phys.* **1980**, *73* (12), 6021.
(27) Huijts, R. A.; Peters, S. M. *Polymer* **1994**, *35* (14), 3119.
(28) Bower, D. I. *J. Polym. Sci., Polym. Phys. Ed.* **1981**, *19*, 93.
(29) van Gurp, M. *Colloid Polym. Sci.* **1995**, *273*, 607.
(30) Pearson, K. *Phil. Trans. A* **1895**, *1860*, 343.
(31) More precisely, H is the full width at half maximum when $f(\theta)$ is defined as a function of θ instead of sin θ. However, for small distribution functions, where $f(\theta) = 0$ for large θ, this approximation is valid since for small θ, sin $\theta \sim \theta$.
(32) Gabriëlse, W.; Angad Gaur, H.; Feyen, F. C.; Veeman, W. S. *Macromolecules* **1994**, *27*, 5811.
(33) Kratky, O. *Kolloid-Z.* **1933**, *64*, 213.
(34) van Wijk, R. J. Personal communication.
(35) Nomura, S. ; Nakamura, N. ; Kawai, H. *J. Polym. Sci. A-2* **1971**, *9*, 407.

MA951693K